Progress In Electromagnetics Research, PIER 33, 1–28, 2001

COMPARISON OF LUEBBERS' AND MALIUZHINETS' WEDGE DIFFRACTION COEFFICIENTS IN URBAN CHANNEL MODELLING

M. Aïdi

Ecole Nationale d'Ingénieurs de Tunis
BP37, Le Belvédère, Tunis, Tunisia

and

Centre d'Etude des Environnements Terrestre et Planétaires
CETP-Vélizy, 10-12 Avenue de L'Europe, 78140 Vélizy, France

J. Lavergnat

Centre d'Etude des Environnements Terrestre et Planétaires
CETP-Vélizy, 10-12 Avenue de L'Europe, 78140 Vélizy, France

Abstract—Luebbers' and Maliuzhinets' solutions for diffraction by a lossy wedge are compared in order to model the urban propagation channel. Derivation, validity criteria and accuracy of impedance boundary conditions (IBCs)—as a main approximation embedded in the Maliuzhinets' solution—are discussed. A modified (a slightly improved) Luebbers diffraction coefficient is proposed. The Uniform Theory of Diffraction (UTD) Maliuzhinets diffraction coefficient is given in a structured form that might facilitate its use. Detailed numerical comparisons of the above-mentioned solutions with method-of-moments solutions using either exact boundary conditions or IBCs are done for canonical configurations.

1 Introduction

2 Impedance Boundary Conditions and Criteria for Their Validity

3 Review of Lossy Wedge Diffraction Coefficients

4 Numerical simulations
4.1 Comparison between the Maliuzhinets and the Luebbers Solutions
4.2 Evaluation of IBCs in RCS of Circular Cylinders Calculations
4.3 Evaluation of the Maliuzhinets and the Luebbers Solutions
5 Synthesis and conclusion
Appendix A.
References

1. INTRODUCTION

The deployment of digital communication systems in urban environments has stressed the need for reliable and accurate wave propagation models. In response to this need, a large number of deterministic models based on ray-tracing techniques and Uniform Theory of Diffraction (UTD) have been proposed in recent years (e.g., [1–3]). To determine ray paths between the base station and the mobile receiver, the most ambitious of these models use data bases that give a detailed description of the urban environment. The propagation of rays and their interactions with buildings, i.e., reflections and lossy wedge diffractions, are calculated by means of the UTD. Encouraging results have been obtained by such approaches and the corresponding models have been found potentially useful as design tools for network planning of cellular systems.

Owing to the complexity of the urban environment, it seems obvious that the viability of such approaches can be reached only with a large amount of assumptions, approximations and speculative simplifications. In other terms, these models are an engineering approach for which:

- Simplifications are necessary and unavoidable,
- Straightforward implemented solutions are often preferred,
- The accuracy of predictions depends on many factors and can be appraised only statistically.

Nonetheless, among the great number of choices that have to be done in the modelling process, it can be reasonably expected that the choice of diffraction coefficients plays a prominent part on the accuracy of predictions. For a lossy diffracting wedge, this choice may be done between two available solutions. The first solution, the

Luebbers' one [4–6], is derived from the results for a perfect conductor wedge and is obtained by a heuristic modification of the diffraction coefficient of Kouyoumjian-Pathak [7]. This solution is easy and straightforward to implement. It has been widely or almost exclusively used for the application considered here. The second solution is the UTD form of the Maliuzhinets diffraction coefficient [8, 9]. The main significant approximation embedded in this second solution is the use of impedance boundary conditions (IBCs) on the faces of the wedge. Otherwise, the Maliuzhinets' diffraction coefficient is more rigorously derived than the Luebbers' one. However, the IBCs seems at first sight questionable in the urban context when they are considered as a high index approximation. In addition, the latter solution is more cumbersome to implement.

The aim of this work is to complete this first analysis by examining in more details the question of the choice between the Luebbers and the Maliuzhinets diffraction coefficients when they are going to be used to model urban channel. Earlier comparisons between Luebbers and Maliuzhinets diffraction coefficients were done by Luebbers [5], Bergljung and Olsson [10] and by Demetrescu et al. [11] for the specific case of urban channel modelling. Although these works give valuable indications, they do not permit to get a clear answer to the addressed problem. Particularly, the results of Demetrescu et al. [11] are overshadowed by the used diffraction coefficient which does not correspond strictly to the one proposed by Luebbers.

The format of this paper reflects the way we have tried to tackle the considered question. Firsts, Section 2 recalls how the IBCs are derived and the criteria of their validity, then their use in urban channel modelling is discussed. Section 3 gives a review of lossy wedge diffraction coefficients. For the Luebbers' diffraction coefficient, the original expression is clearly stated and a modified formulation is proposed. For the UTD form of the Maliuzhinets coefficient, the coefficient is expressed in a structured form which should facilitate its use. Finally, slope diffraction coefficients are also considered. Section IV presents different numerical simulation results. First, Luebbers and Maliuzhinets formulations are numerically compared for a single wedge configuration. Next, the criteria of validity of IBCs are examined by comparing radar cross section results for circular cylinders. In this comparison, both the solutions with exact boundary conditions and with approximate IBCs are based on the method of moments (MoM). Finally, Luebbers and Maliuzhinets results for diffraction by a square cylinder are compared to MoM results. All these simulations are done with data that are representative of the urban context. Section V gives a synthesis and our conclusions.

2. IMPEDANCE BOUNDARY CONDITIONS AND CRITERIA FOR THEIR VALIDITY

Impedance boundary conditions (IBCs) where first introduced by Leontovich [12] (1948) in works related to the study of radiowave propagation over the earth. In scattering problems, they enable to solve the exterior problem for the field outside the scatterer independently of the internal field. This is their main attractive characteristic and such approximate boundary conditions have been since widely studied and used. The main references to works on IBCs can be found in Senior's papers [13, 14].

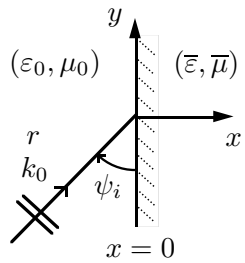

Figure 1. Reflection at a plane interface.

The most common of these IBCs can be derived by considering the simple canonical problem of reflection of a plane wave incident on a homogenous half-space. Using the notations sketched in Figure 1, the classical solution of this problem permits to establish the following relations at the interface ($x = 0$):

$$\frac{1}{Z_0}(E_y/H_z) = \sin(\theta_{+1}), \qquad -\frac{1}{Z_0}(E_z/H_y) = \sin(\theta_{-1}) \tag{1}$$

where

$$\sin(\theta_p) = \sin(\theta_p^c)\left(1 - \cos^2(\psi_i)/\bar{N}^2\right)^{1/2} \quad \text{for} \quad p = \pm 1. \tag{2}$$

In these last equations, Z_0 is the free space impedance, $\bar{N}$ denotes the refractive index of the material in the half-space ($\bar{N} = \sqrt{\bar{\varepsilon}\bar{\mu}}$) and ψ_i is the incidence angle; the parameter $\sin(\theta_p^c)$ is related to the polarization $p = \pm 1$ and to the complex relative constitutive parameters of the half-space $(\bar{\varepsilon}, \bar{\mu})$ through the relation:

$$\sin(\theta_p^c) = (\bar{Z})^p = \left(\sqrt{\frac{\bar{\mu}}{\bar{\varepsilon}}}\right)^p. \tag{3}$$

Invoking energy considerations, the square roots in (2) and (3) are determined such that the real parts of $\sin(\theta_p^c)$ and $\sin(\theta_p)$ are positive. In the sequel of this paper, subscripts p will be dropped. The two polarization cases (H_z ($p = +1$) and E_z ($p = -1$)) are treated together and all the expressions apply to both cases provided that the proper value for $\theta^c_{+1,-1}$ is used.

To apply the IBCs (1) to a homogeneous body of finite size immersed in free space, some restrictions must be introduced. The body surface must be smooth and the minimum radius of curvature a of the body must be large compared to the wavelengths in the material and in the surrounding free space. In other respects, the resulting IBCs will be particularly effective and helpful only if they uncouple the resolution of the problem for the exterior free space field from that for the field inside the body. To meet this condition, the body material must be lossy and the penetration depth δ must be small compared to a. Defining the two parameters (w_a, q_0) by

$$w_a = \frac{\delta}{a} = \left|\mathrm{Im}(\bar{\mathrm{N}})\right| k_0 a, \qquad q_0 = \frac{1}{k_0 a}, \tag{4}$$

the above restrictions can be expressed by

$$w_a \gg 1 \tag{5}$$

$$q_0 \ll 1 \tag{6}$$

High frequency approximation

Through the parameter $\sin(\theta)$ defined in (2), the IBCs (1) are dependent of the incident field direction ψ_i. Therefore, their main practical applicability rests on the use of rays methods such as the UTD. However, this requirement seems to be reasonable since it falls into line with the imposed high frequency condition (6). This first case will be referred to as 'high frequency IBC' (HF IBC) or 'variable impedance' (Zv IBC). For numerical methods such as the moment method, one can expect that the use of this HF IBC will be generally restricted to convex bodies.

High refractive index approximation

On another hand, for a high refractive index ($\left|\bar{N}\right| \gg 1$), $\sin(\theta)$ given in (2) can be approximated by $\sin(\theta) \approx \sin(\theta^c)$. The IBCs (1) become then independent of the incident field direction ψ_i. Moreover, by a different asymptotic analysis for which the small parameter is $1/\bar{N}$, it can be shown [14] that the high frequency condition (6) can be relaxed for the case of high refractive index. Then two restrictions

remains:

$$w_a \gg 1, \qquad |\bar{N}| \gg 1. \tag{7}$$

This second case will be referred to as 'high index IBC' (HI IBC) or 'constant impedance' (Zc IBC).

To sum up and to gather the two cases, requirements ((5), (6), and (7)) for the validity of the IBCs can be replaced by:

$$w_a \gg 1, \tag{8}$$

$$q = \frac{q_0}{|\bar{N}|} \ll 1. \tag{9}$$

For low $|\bar{N}|$, q_0 must be $\ll 1$ and the IBCs depend on ψ_i. For ($|\bar{N}| \gg 1$), (2) can be simplified to $\sin(\theta) \approx \sin(\theta^c)$ and the restriction imposed by the two conditions ((8) and $|\bar{N}| \gg 1$) on the magnitude of q_0 can be viewed as a sufficient condition to drop away (9). Therefore the HI IBC can be regarded as a particular approximation simplifying the HF IBC.

When the surface of the diffracting body is irregular, it is commonly assumed that IBCs still generate accurate results; the parameter a has to be redefined then as a minimum characteristic thickness of the body. For example, the applicability of IBCs for bodies with curved edges was confirmed by Huddleston [15] by a series of tests for finite conducting cylinders with thin coatings.

From a practical point of view, more clearly defined criteria for the HI case were obtained by Wang [16] on the ground of theoretical analyses and numerical simulations. These are:

$$w_a \geq 2.3, \tag{10}$$

$$|\bar{N}| \geq 10, \tag{11}$$

in order to keep ≈ 1 percent error (i.e., 0.09 dB) in the predictions of the radar cross section of a scattering body at all scattering directions. Then ($q \leq 1/2.3$) and therefore the criterion (9) can be considered as automatically fulfilled. To the best of our knowledge, we have not found in the literature, such similar indications about the practical interpretation of the conditions (8), (9) for the HF case.

Impedance boundary conditions and urban channel

For radiowave propagation modelling, urban environments and connected recent communication systems correspond roughly to the following set of electromagnetic parameters (frequency band $f \approx 0.9$ to 3 GHz, material characteristics of urban constructions: $\varepsilon_r \approx 3$ to 10, $\mu_r \approx 1$, $\sigma \approx 10^{-3}$ to 10^{-2} S/m). The characteristic

length a of the main scatterers (buildings) present in urban scenes counts in tens meters ($a \approx 10$ m).

With this range of data, which will be used in all the sequel of this paper, w_a and $|\bar{N}|$ can be approximated by

$$w_a \approx 60\pi \frac{a\sigma}{\sqrt{\varepsilon_r}}, \qquad |\bar{N}| \approx \sqrt{\varepsilon_r}. \tag{12}$$

Thus, we can make the following remarks:

- $(1.7 \leq |\bar{N}| \leq 3)$ so that the validity of the HI IBC is questionable. However, the HI IBC cannot be definitely rejected as the error demand of 0.09 dB used to establish the conditions (10) and (11) may be thought excessive in the context of urban channel modelling.
- w_a is approximately independent of the frequency and, with regard to the conditions (10) and (11), w_a increases as ε_r (or $|\bar{N}|$) is decreased.
- The criterion $w_a \geq 2.3$ is rather well satisfied; in the 'worst case' ($\varepsilon_r = 10$, $\sigma = 10^{-3}$ S/m) we must have $a \approx 40$ m to meet this criterion.
- q_0 and q are of the same order of magnitude and they verify (q_0 and $q < 0.05/a$). Hence, we always have (q_0 and q $\ll 1$) . Nevertheless, without a precise statement of the practical interpretation of the condition (9), we cannot assert that this criterion (9) is fulfilled.

Consequently, it seems that complementary numerical simulations are required to examine the accuracy of the IBC when used in the context of urban channel modelling. This will be done in Section 4.

3. REVIEW OF LOSSY WEDGE DIFFRACTION COEFFICIENTS

Classical and obvious notations for the problem of diffraction by a wedge of exterior angle $N\pi$ are sketched in Figure 2. The faces of the wedge are referenced as 0 face and N face. The complex relative constitutive parameters of the lossy wedge are denoted by $(\bar{\varepsilon}, \bar{\mu})$ and the wavenumber in the free space surrounding the wedge is denoted by k. We restrict ourselves to normal incidence and the edge of the wedge is taken as z axis. The wedge is illuminated by a line source located at (s_0, φ_0) and the field is observed at a point m located at (s, φ) where the angles φ_0 and φ are measured with respect to the reference 0 face (cf. Fig. 2). The transverse magnetic ($U = H_z$, $p = +1$) and the transverse electric ($U = E_z$, $p = -1$) polarization cases are treated together.

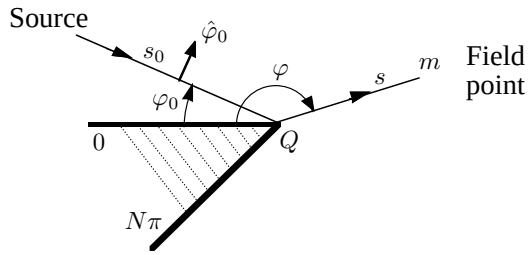

Figure 2. Wedge diffraction.

Luebbers' heuristic diffraction coefficient

The Luebbers' diffraction coefficient for a lossy wedge [4] was obtained by modifying heuristically the perfect conductor UTD diffraction coefficient of Kouyoumjian-Pathak [7]. The approach is to introduce reflection coefficients in Kouyoumjian-Pathak's results to compensate discontinuities of the geometrical optical field at the reflection shadow boundaries. With the assumption that propagation through the wedge can be neglected, the resulting diffraction coefficient for a lossy wedge is written as:

$$D = h(\phi^i) + h(-\phi^i) + R^N(\psi_N) \cdot h(\phi^r) + R^0(\psi_0) \cdot h(-\phi^r) \qquad (13)$$

where $(\phi^i = \varphi - \varphi_0,\ \phi^r = \varphi + \varphi_0)$ and the definition of the function h is recalled in Appendix A. For the normal incidence case considered here, the two real parameters $(kL,\ N)$ needed to calculate h are defined by:

$$(kL = \sqrt{\frac{k\,s_0\ k\,s}{k\,s_0 + k\,s}},\ N = \text{the wedge angle parameter}). \qquad (14)$$

Also, R^0 and R^N are the reflection coefficients for the 0 face and for the N face. When roughness is not considered, these are simply given by

$$R^\ell(\psi) = \frac{\sin(\psi) - \sin(\theta_\ell)}{\sin(\psi) + \sin(\theta_\ell)} \qquad (\ell = 0, N) \qquad (15)$$

with $\sin(\theta_\ell)$ calculated as in (2). To complete this construction, it remains to define the arguments (ψ_0, ψ_N) of the two reflection coefficients appearing in (13). This is done somewhat arbitrarily with mainly two requirements.

First, the arguments (ψ_0, ψ_N) must be chosen such as to compensate discontinuities of the geometrical optical field at the reflection shadow boundaries:

$$R^0(\psi_0) = R^0(\varphi_0) \text{ when } \varphi + \varphi_0 = \pi$$

$$R^N(\psi_N) = R^N(N\pi - \varphi_0) \text{ when } (\mathrm{N}\pi - \varphi) + (\mathrm{N}\pi - \varphi_0) = \pi \quad (16)$$

Second, a much more important requirement, often wrongly neglected, the overall construction must produce 'good predictions'!

In this work, we will consider two different choices given by:

$$\text{Luebbers choice} : \begin{cases} \psi_0 = \mathrm{Min}(\varphi_0, \varphi) \\ \psi_N = \mathrm{Min}(N\pi - \varphi_0, N\pi - \varphi) \end{cases} \quad (17)$$

$$\text{Modified choice} : \{\psi_0 = \psi_{\mathrm{N}} = \mathrm{Min}(\varphi_0, \varphi, \mathrm{N}\pi - \varphi_0, \mathrm{N}\pi - \varphi) \quad (18)$$

The first set is simply obtained by extending the Luebbers' definitions (Luebbers assumes $\varphi_0 < \varphi$ in his papers) to arbitrary (φ_0, φ) by taking into account the necessary invariance of the diffraction coefficient relatively to the arbitrary choice of the reference 0 face.

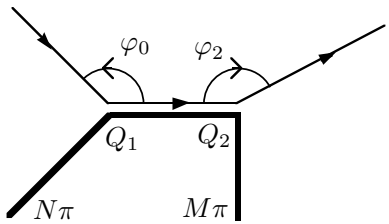

Figure 3. Double wedge diffraction.

To explain the motivations of the modified choice, let us analyze the diffraction by a double wedge structure as shown in Figure 3. For an incident field U^i, the ray simply diffracted by Q_1 is given by:

$$U_1^d(m) = D(\varphi, \varphi_0)\, U^i(Q_1)\, \frac{\exp(-jks)}{\sqrt{ks}} \quad (19)$$

At grazing observation direction $\varphi = 0$ (i.e., over the face Q_1Q_2), this ray represents, for the treatment of its re-diffraction by Q_2, a total field, sum of an incident part $\tilde{U}^i$ and a reflected part $\tilde{U}^r$:

$$\text{for } \varphi = 0 : \quad U_1^d = \tilde{U}^i + \tilde{U}^r = (1 + R)\tilde{U}^i \quad (20)$$

As the reflection coefficient ($R = -1$) at grazing incidence and $\tilde{U}^i$ cannot be infinite, we must have:

$$D(0, \varphi_0) = 0 \quad (21)$$

and $\tilde{U}^i$ remains undetermined.

It is a simple matter to show that then $D(\varphi_2, 0) = 0$ so that the indetermination of $\tilde{U}^i$ at Q_2 is not puzzling as $\tilde{U}^i$ gives null re-diffraction.

The modified choice has been introduced to satisfy this requirement of null diffraction coefficient for grazing incidence:

$$D(\varphi, 0 \text{ or } \mathrm{N}\pi) = \mathrm{D}(0 \text{ or } \mathrm{N}\pi, \varphi) = 0. \tag{22}$$

In Section 4 of this paper, we will see that this choice yields a slight improvement of predictions in comparison with the Luebbers' choice.

Finally, let us notice that the non explicitly mentioned choice made by Demetrescu et al. in their work [11] was $(\psi_0 = \varphi_0, \psi_N = N\pi - \varphi_0)$. This latter choice is a misinterpretation of the Luebbers' formulation and is inadequate as observed by Demetrescu et al.

Maliuzhinets diffraction coefficient

The UTD form of the Maliuzhinets diffraction coefficient for impedance wedge was established by Tiberio et al. in [8] for the case of an incident plane wave and generalized in [9] for a line source illumination. As noticed by James [17], it is rather simple to extend heuristically the results of [8] to a general astigmatic incident wave. However, the diffraction coefficient of [9] is to be preferred to the [8]'s one. Indeed, the two results have equivalent complexity but the [8]'s one does not exhibit reciprocity with respect to the directions of incidence and observation (though numerically this defect is limited to a very narrow domain rather difficult to detect, e.g., around $(\varphi, \varphi_0) = (0, \pi)$).

To recall the results of [9] in a form that should make their use easier, we found more convenient to move from the $\theta_{0,N}$ impedance parameters of the wedge faces to the notation:

$$\nu_{0,N} = \frac{\pi}{2} - \theta_{0,N} \tag{23}$$

and to introduce the two auxiliary parameters

$$\begin{aligned} c_1 &= \cos\left(\frac{\nu_0}{N}\right)\cos\left(\frac{\nu_N}{N}\right) - \cos^2\left(\frac{\pi}{2N}\right) \\ c_2 &= \frac{1}{2\sin\left(\frac{\pi}{2N}\right)}\left(\cos\left(\frac{\nu_0}{N}\right) - \cos\left(\frac{\nu_N}{N}\right)\right) \end{aligned} \tag{24}$$

For the high index IBC, (c_1, c_2) are wedge characteristics. For the high frequency IBC, they also depend on the illumination angles (ψ_0, ψ_N)

of the wedge faces 'near' the edge of the wedge. For a shadowed face ψ is equal to zero.

With these notations and the same definitions as above for $(\phi^i, \phi^r, h, kL, N)$, the Maliuzhinets diffraction coefficient is given by:

$$D(\varphi,\varphi_0) = \Omega_N(\varphi,\varphi_0)\cdot\Big\{+A_N(u,-u_0)\,h(+\phi^i) + A_N(-u,u_0)\,h(-\phi^i) \\ -A_N(u,u_0)\,h(+\phi^r) - A_N(-u,-u_0)\,h(-\phi^r)\Big\} \tag{25}$$

in which

$$u_0 = \sin(\varphi_0/N), \qquad u = \sin(\varphi/N), \\ A_N(x,y) = c_1 - x\,y - c_2(x+y) \tag{26}$$

and where $\Omega_N(\varphi,\varphi_0)$ is related to the renormalized Maliuzhinets function $\overline{\psi}_N(\alpha)$ through the relations:

$$\Omega_N(\varphi,\varphi_0) = \frac{1}{4\,\psi(\varphi)\,\psi(\varphi_0)}, \\ \psi(\alpha) = \overline{\psi}_N(\alpha+\nu_N)\overline{\psi}_N(\alpha-\nu_N)\bar{\psi}_N(N\pi-\alpha+\nu_0)\overline{\psi}_N(N\pi-\alpha-\nu_0). \tag{27}$$

Definition of the Maliuzhinets function $\overline{\psi}_N(\alpha)$ and efficient algorithms for its numerical approximation can be found in [18].

Finally, it should be observed that, since the Maliuzhinets solution is established for a wedge with a constant impedance on each face, the use of these results is heuristic for the high frequency IBC when a line source excitation is considered.

Slope diffraction coefficients

When expression (19) predicts a null diffracted field, a better approximation of the diffracted field can be obtained by including the so-called slope diffraction term [17]. For the perfect conducting case, this slope diffracted field can be written as:

$$U^{sd}(m) = D^s\cdot\left(\frac{1}{k}\frac{\partial U^i(m)}{\partial\hat{\varphi}_{\mathbf{0}}}\right)_{m=Q}\frac{\exp(-jks)}{\sqrt{ks}} \tag{28}$$

where $\hat{\varphi}_{\mathbf{0}}$ is the orthoradial vector sketched in Figure 2 and the slope diffraction coefficient D^s is given by

$$D^s = -j\frac{\partial D}{\partial\varphi_0}. \tag{29}$$

It is customary to extend heuristically this result to the dielectric wedge case.

Luebbers heuristic slope diffraction coefficient

In a rather obscure paper, Luebbers [6] has proposed a heuristic slope diffraction coefficient starting from the set (17) as definition of (ψ_0, ψ_N). It is a simple matter to show that the modified second set (18) leads to a clear construction of the slope diffraction coefficient by a straightforward application of (28), (29). Nonetheless, the resulting coefficient will not be given here as we have experienced that it is not reliable definitively.

Maliuzhinets slope diffraction coefficient

Due to the occurrence of the $\Omega_N(\varphi, \varphi_0)$ function in (25), the calculation of Maliuzhinets slope diffraction coefficient for general values of (φ, φ_0) is a hard task. However, the slope diffraction gives a significant contribution mainly for the specific situation depicted in Figure 2, i.e, for the doubly diffracted field by a double wedge structure. We can then restrict ourselves to the case (φ, $\varphi_0 = 0$ or Nπ) for which there is no more needs to calculate $\Omega_N(\varphi, \varphi_0)$ derivative to obtain D^s as $D(\varphi,\ \varphi_0 = 0 \text{ or } \mathrm{N}\pi) = 0$. The resulting Maliuzhinets slope diffraction coefficient is

For $\varphi_0 = qN\pi$ (with q = 0 or 1)

$$D^s(\varphi,\varphi) = 2\Omega_N(\varphi,\varphi_0)\Big\{(c_1 + c_2\,u)\,hs(-\phi^r) + (-c_1 + c_2\,u)\,hs(+\phi^r) + (-1)^{q+1}\frac{j}{N}\Big((u - c_2)\,h(-\phi^r) + (u + c_2)\,h(+\phi^r)\Big)\Big\} \quad (30)$$

where the function hs is defined in Appendix and the other notations are as before. Finally, it can be useful to notice the relationship:

$$\partial_1 D(\varphi_0,\varphi) = jD^s(\varphi,\varphi_0) \quad (31)$$

(∂_1 derivative relatively to the first argument),

which is also needed in the determination of the doubly diffracted field by a double wedge structure.

4. NUMERICAL SIMULATIONS

General considerations

We evoke here various general considerations.

As mentioned in the introduction, for urban channel models, a 'point to point comparison' between results has little meaning; the

comparisons have to be done statistically. This justifies the statistical parameters that we will introduce farther on. Among these parameters, it must be observed that the maximum error is irrelevant in most of the cases.

On another hand, for simple canonical configurations such as those considered farther on (single wedge, square cylinder), it seems to us that the single comparison of total fields is insufficient. Indeed, due to shadowing effects, for a given wedge interaction in the actual situation of an urban environment, the incident ray, the reflected ray and the diffracted ray can potentially separately contribute to the total field. To take partially into account this remark, analysis will be carried out both for total fields and for diffracted rays fields. It should be observed here that the Luebbers and Maliuzhinets solutions use the same geometrical optics field $U^{GO} = U^i + U^r$ so that they differ only in their diffracted rays fields.

Before tackling the evaluation of the Luebbers and the Maliuzhinets solutions, it would be interesting to guess the accuracy demand upon a single interaction which is needed by our intended application. This is a rather impossible task. Let us recall first some properties of existing models in macro-cellular context. For median path loss, in better cases, the statistical comparison of predictions of models and measurements yields generally a standard deviation of ≈ 10 dB [11]. On another hand, only paths with a limited number of diffractions (generally $\leq 4 \sim 6$) are computed by models. Taking into account these two last facts, we guess on absolute speculation that keeping the mean error less than ≈ 1 dB for the simple canonical cases considered hereafter might be sufficient to get satisfactory results when the urban case is invoked.

4.1. Comparison between the Maliuzhinets and the Luebbers Solutions

We will illustrate the comparison between the Maliuzhinets with HF IBC and the Luebbers solutions by considering the configuration sketched in Figure 4a. Figure 4b depicts the comparison of total fields and diffracted rays fields calculated by the Maliuzhinets approach and the Luebbers approach. The top graph gives the total fields and the diffracted rays fields for the three solutions (Maliuzhinets, Luebbers and modified Luebbers). The middle and the bottom graphs give differences between the two Luebbers type solutions and the Maliuzhinets solution when total fields (middle graph) or diffracted rays fields (bottom graph) are considered. All the differences are differences between fields expressed in dB.

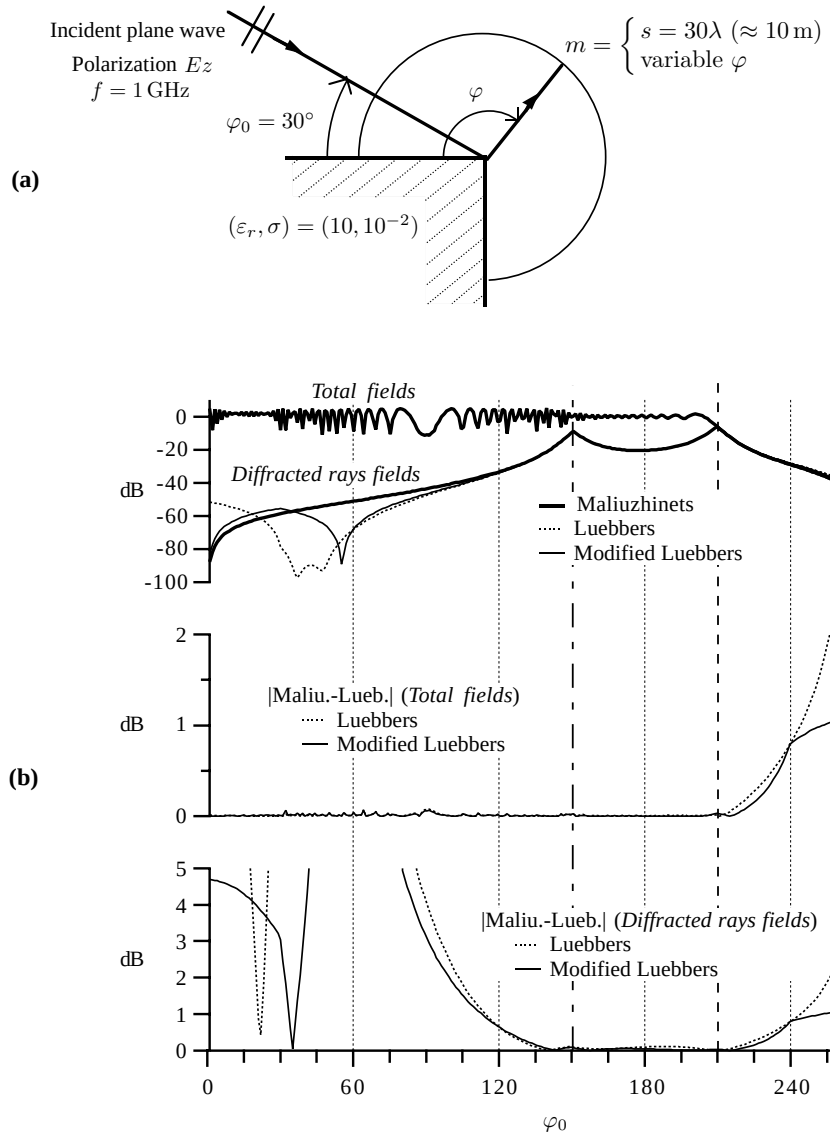

Figure 4. a) Configuration used for the comparison Luebbers/Maliuzhinets. b) Comparison of Luebbers, modified Luebbers and Maliuzhinets solutions. HF IBC is used. (Vertical dashed lines correspond to shadow boundaries).

From this figure (*and many other calculations*), we can draw the following conclusions (*most of them are already known* [5, 10, 11]):

- Almost everywhere for the total field and near shadow boundaries for the diffracted rays field, Maliuzhinets and Luebbers results are indistinguishable.
- For the diffracted rays field, outside the vicinity of shadow boundaries, Luebbers' results are not reliable. Nevertheless it should be observed that the preponderant diffracted rays in magnitude are obtained near shadow boundaries.
- The modified Luebbers formulation (18) gives a slight improvement of the original one.

In other terms, Luebbers approach can be considered as an approximation of the Maliuzhinets one. With these conclusions, it seems to us that the original question of the choice of the diffraction coefficients is better expressed as: 'Is the widely used and less cumbersome Luebbers approximation sufficiently accurate for the urban channel modelling purpose?'

4.2. Evaluation of IBCs in RCS of Circular Cylinders Calculations

In this section, we shall examine the validity of IBCs in RCS of circular cylinders calculations. More precisely, our aim is limited to get some indications about the criteria of validity and accuracy of the IBCs in the particular context of the urban channel modelling. For that purpose, we will compare method-of-moments solutions (MoM) using either exact boundary conditions, HI IBC or HF IBC. These three cases will be referred to by (D, Zc, Zv).

Presentation

As an introductory example, we shall consider the case of a circular cylinder of radius $a = 15\lambda$ illuminated by an H_z-polarized plane wave with ($f = 0.9$ GHz, $\varepsilon_r = 3$, $\sigma = 0.01$ S/m). Figure 5 displays:

- The comparison of the three RCS in dB: $RCS(D)$, $RCS(Zc)$, $RCS(Zv)$ (top graph)
- The error curves (middle graph):
  $$DZc = |RCS(D) - RCS(Zc)|$$
  $$DZv = |RCS(D) - RCS(Zv)|$$
- The associated cumulative distribution functions of errors (bottom graph) and the related statistical parameters ($Emax$: maximum error, $Eavg$: average error, $Esdev$: standard deviation,

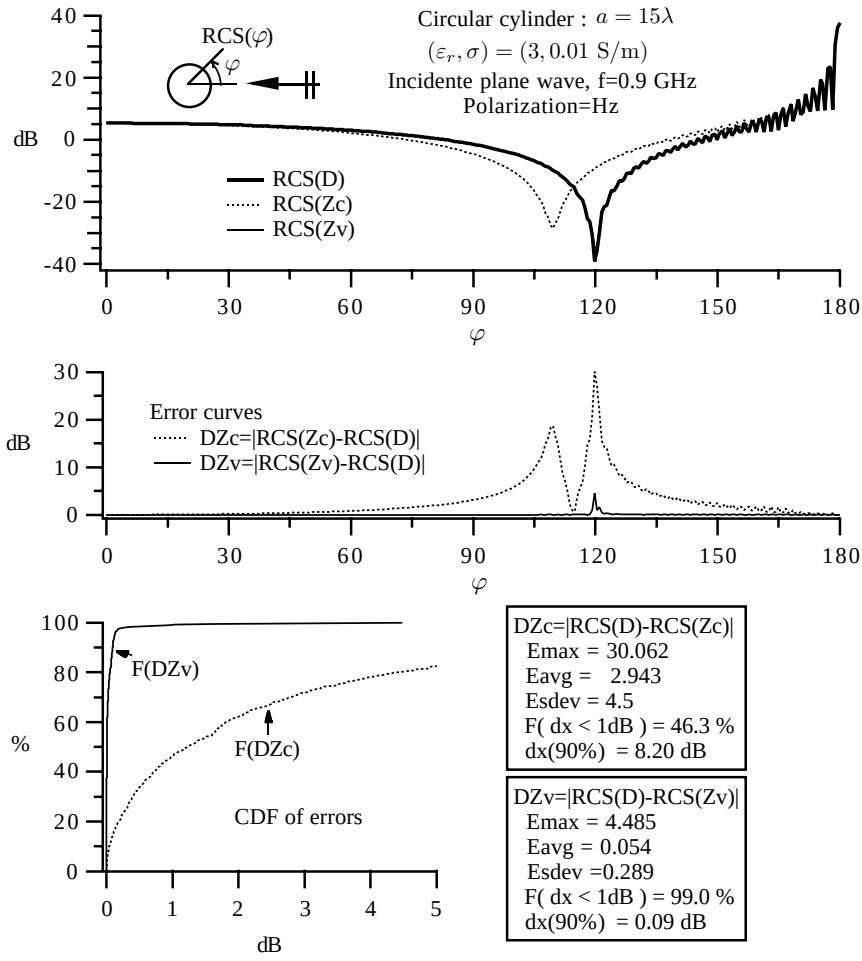

Figure 5. RCS of a circular cylinder: evaluation of the validity of the IBCs.

$F1dB$=F($dx \leq$1dB) percentage of errors lower than 1 dB, $dx(90\%)$: error at 90%).

This Figure 5 shows that the Zv IBC gives excellent results. In contrast, the Zc IBC produces good results only for forward and backward directions. From our extensive simulations, for the Zc IBC validity, the presented case can be qualified as one of the worst cases.

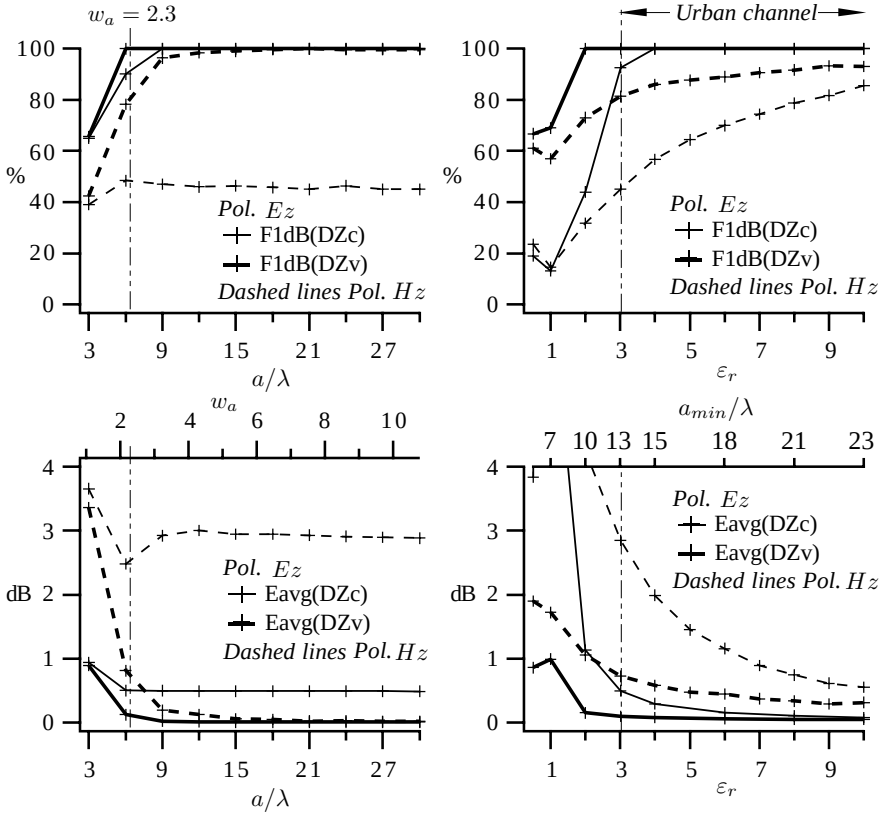

Figure 6. For $f = 0.9$ GHz. Variation of the statistical parameters $(Eavg,\ F1dB)$ in calculating RCS of circular cylinders:
- Left: as a function of the normalized radius a/λ of the cylinder for $(\varepsilon_r, \sigma) = (3, 10^{-2}\ \text{S/m})$
- Right: as a function of the relative permittivity ε_r for $\sigma = 0.005$ S/m and $w_a = 2.3$ (i.e., $a = a_{min}$).

Study of the w_a criterion versus the cylinder radius

With the same data ($f = 0.9$ GHz, $\varepsilon_r = 3$, $\sigma = 0.01$ S/m), similar analyses were performed with various cylinder radii ranging from 3λ to 30λ (i.e., for various w_a). The left graphics of Figure 6 give the resulting variations of the two statistical parameters $(Eavg, F1dB)$ versus the normalized cylinder radius a/λ. The main lessons that can be drawn form that curves are:

- When $w_a > 2.3$, the Zv IBC results can be qualified as rather satisfactory for the urban channel modelling purpose.

- The single condition $w_a > 2.3$ seems to be a pertinent criterion for the validity of the Zv IBC, at least for the considered set of data.
- For the case (H_z polarization/Zc IBC), it seems that increasing w_a doesn't permit to reduce the error DZc.

Study of the w_a criterion versus the permittivity

With ($f = 0.9$ GHz, $\sigma = 0.005$ S/m), similar analyses were performed at various permittivities ε_r and constant $w_a = 2.3$, i.e., with the cylinder radius $a = a_{mim}$ fixed by the condition $w_a = 2.3$. The right graphics of Figure 6 give the resulting variations of the two statistical parameters ($Eavg$, $F1dB$) versus the cylinder permittivity ε_r.

For ε_r in [3, 10], we get a confirmation that, with the single criterion $w_a > 2.3$, the Zv IBC yields rather satisfactory results for the urban channel modelling purpose (say to keep average error below ≈ 1 dB). For $\varepsilon_r < 3$, we have experienced, from a few simulations not presented here, that the results given in Figure 6 can be improved by increasing w_a. In other terms, for $\varepsilon_r < 3$, the Zv IBC seems to remain valid but with a more stringent limitation on w_a. Since this case is outside the range of parameters considered in this work, it has not been explored further.

Figure 6 shows also that the discrepancy between the exact BC and the Zc IBC results decreases with increasing ε_r. Except for the case (H_z polarization, low ε_r), the Zc IBC results, though less satisfactory than the Zv IBC ones, can be judged adequate for the urban channel modelling purpose again with the conditions $\varepsilon_r > 3$ and $w_a > 2.3$. In other respects, it can be inferred that, for the urban channel, the main contributing paths are those for which interactions correspond either to forward diffractions or/and to 'near shadow boundary' diffractions. Consequently, referring again to the Figures 4 and 5, it can be thought that, even for the exception case (H_z polarization, low ε_r), the observed discrepancies are not so significant for the intended application.

4.3. Evaluation of the Maliuzhinets and the Luebbers Solutions

In this part, for the Luebbers approach, only the modified formulation will be examined.

To illustrate general trends of the Maliuzhinets and the Luebbers solutions, we shall consider the diffraction by a square cylinder of

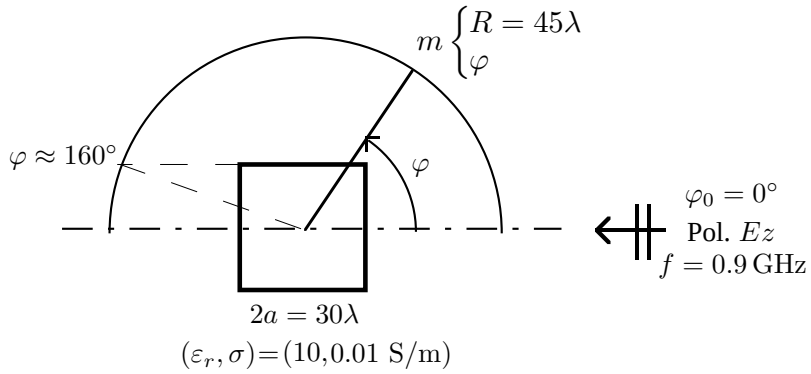

Figure 7. Configuration used to evaluate Luebbers and Maliuzhinets solutions.

side $2a = 30\lambda$ (*a building of characteristic length* $\approx$ 10 m) with ($f = 0.9$ GHz, $\varepsilon_r = 10$, $\sigma = 0.01$ S/m), and an E_z polarization (then $w_a \approx 3$). The fields will be observed at a finite distance over the co-centric circle of radius $R = 45\lambda$ with a resolution of 5 points per free space wavelength. To evaluate the potential benefits and the limitations provided by retaining slope diffraction terms, we shall consider the case of a grazing incidence angle $\varphi_0 = 0°$ (cf. Figure 7). This case involves the well-known UTD-problem of overlapping transition zones [17]. Analysis will be done both for total fields and for diffracted rays fields. For the results based on the method of moments, the diffracted rays field is defined and calculated by the coherent difference between the total field and the geometrical optical field.

To be able to evaluate the extent to which the accuracy of IBCs is affected by edges, we first take, as a reference case, the same configuration with the square cylinder simply replaced by a circular cylinder of radius $a = 15\lambda$. The results for this reference case are given in Figure 8 in which the $MoM(D)$ and the $MoM(Zv)$ solutions are compared. For this Figure 8, it should be remarked that one has to take some cautions in the interpretation of the error curves, which is true for all the results presented in this paper. Indeed, a certain amount of error is due to a loss of numerical precision or numerical artifacts. This may occur when the field has rapid variations. This also happens for low diffracted rays fields when they are calculated as a difference. The results of this reference case will be discussed together with those of the next case.

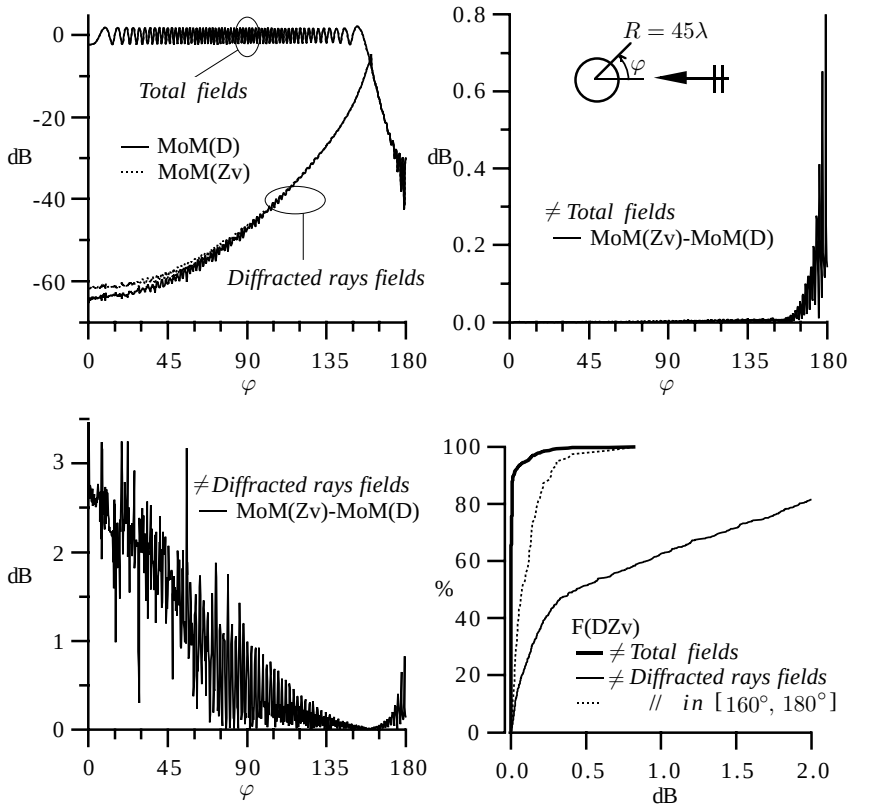

≠ Total fields	≠ Diffracted rays fields	≠ Diffracted rays fields in [160°, 180°]
Emax = 0.83	Emax = 3.466	Emax = 0.83
Eavg = 0.016	Eavg = 0.88918	Eavg = 0.119
Esdev = 0.059	Esdev = 0.91343	Esdev = 0.137
F(dx < 1dB) = 100.0 %	F(dx < 1dB) = 62.5 %	F(dx < 1dB) = 100.0 %
dx(90%) = 0.02 dB	dx(90%) = 2.32 dB	dx(90%) = 0.27 dB

Figure 8. Diffracted field by a circular cylinder ($a = 15\lambda$) calculated over the circle $R = 45\lambda$. Evaluation of the validity of the HF IBC for finite distance field calculations. (Pol. E_z, $f = 0.9$ GHz, $\varepsilon = 10$, $\sigma = 0.01$ S/m).

In the analysis of the square cylinder case, we will distinguish the illuminated region [0°, ≈ 160°] from the shadowed region [≈ 160°, 180°].

Illuminated region [0°, ≈ 160°]

For the illuminated region, Figure 9 shows a comparison of the three following solutions:

- $MoM(Zv)$: MoM solution using the Zv IBC,
- $Maliu$: UTD solution using the Zv IBC and the Maliuzhinets diffraction coefficient,
- $Lueb$: UTD solution using the modified Luebbers diffraction coefficient,

with the reference solution:

- $MoM(D)$: MoM solution using exact boundary conditions.

For all the UTD results, only singly-diffracted rays are taken into account. From this Figure 9 and from its comparison with Figure 8, we can draw the following key trends:

- The edges do not seem to have any significant impact on the validity of IBCs. This result has been also observed by Huddleston [15] for curved edges for the HI IBC.
- For total field predictions, all the results ($MoM(D)$, $MoM(Zv)$, $Maliu$, $Lueb$) are almost indistinguishable.
- For diffracted rays field predictions:
  - $MoM(Zv)$ and $Maliu$ results give almost the same errors relatively to the $MoM(D)$ solution. The Maliuzhinets solution is then a very good approximation of the $MoM(Zv)$ one and the main error in these two solutions is mainly related to the use of the IBC. Other calculations, not shown here, indicate that the $Maliu$ results can be slightly improved near the shadow boundary ($\varphi_0 \approx 160°$) by including doubly diffracted rays with slope diffraction.
  - The $Lueb$ solution gives larger errors than the $Maliu$ one, though these errors are less important than would be expected from the first comparison for a single wedge (subsection A). In the forward direction (say φ_0 in [90°, 160°]), $Lueb$ and $Maliu$ predictions have almost the same degree of error.

A series of calculations have been done for other angles of incidence. When the incident field is not at grazing incidence, no problem of overlapping transition zones occurs and the analyses have been carried out over all the interval [0°, 360°]. These calculations showed that the

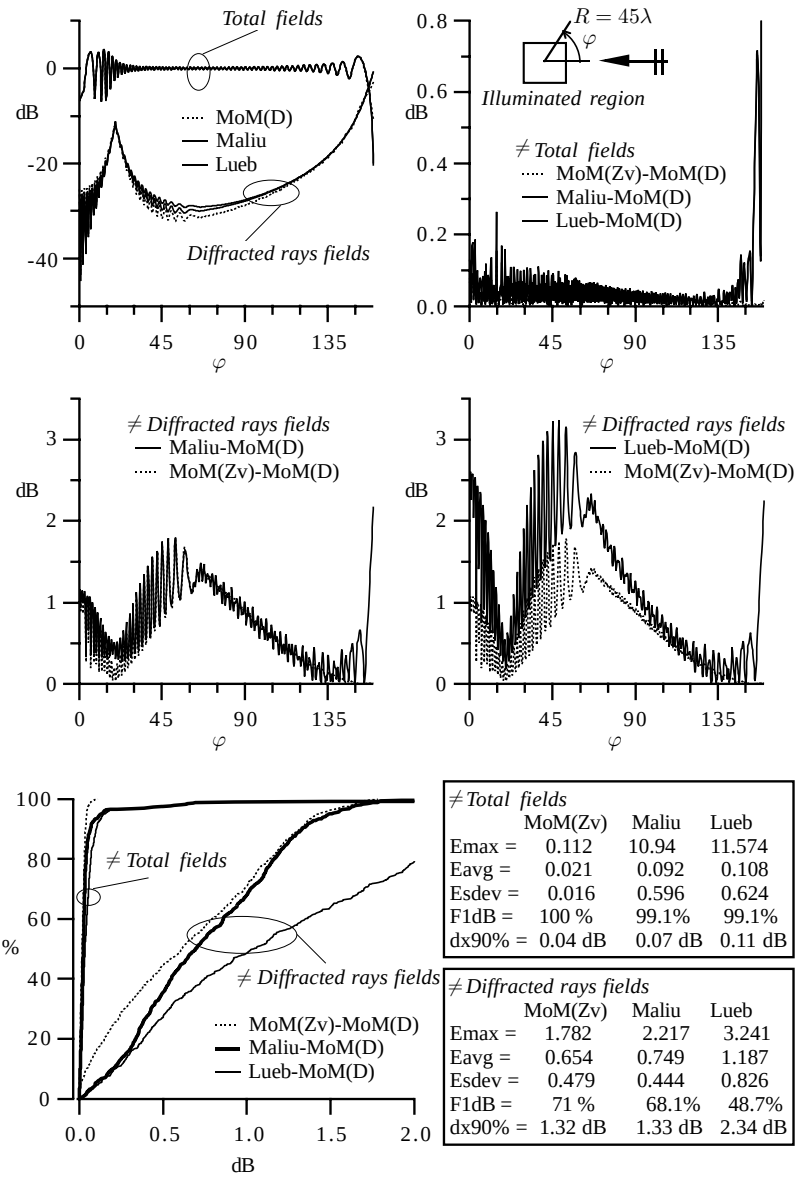

≠ Total fields	MoM(Zv)	Maliu	Lueb
Emax =	0.112	10.94	11.574
Eavg =	0.021	0.092	0.108
Esdev =	0.016	0.596	0.624
F1dB =	100 %	99.1%	99.1%
dx90% =	0.04 dB	0.07 dB	0.11 dB

≠ Diffracted rays fields	MoM(Zv)	Maliu	Lueb
Emax =	1.782	2.217	3.241
Eavg =	0.654	0.749	1.187
Esdev =	0.479	0.444	0.826
F1dB =	71 %	68.1%	48.7%
dx90% =	1.32 dB	1.33 dB	2.34 dB

Figure 9. Diffracted field by a square cylinder (half side $a = 15\lambda$) calculated over the circle $R = 45\lambda$. Illuminated region. Evaluation of the validity of the HF IBC and comparison with UTD results (see Figure 7 for the definition of the configuration). UTD results ($Lueb, Maliu$) include only simply diffracted rays.

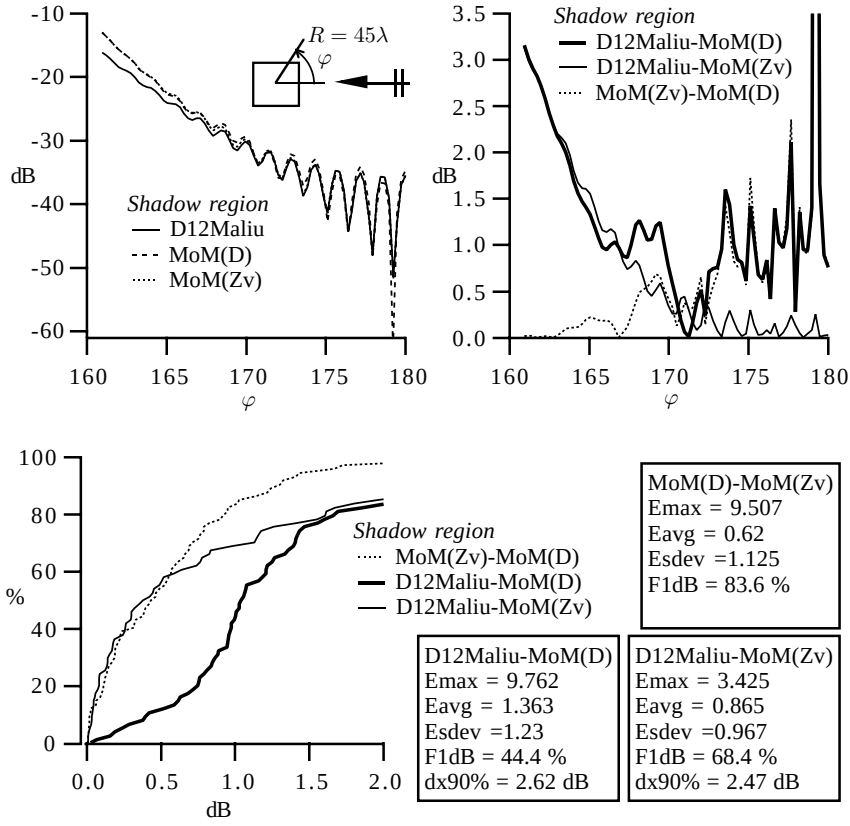

Figure 10. As Figure 9 but for the shadow region. UTD results ($D12Maliu$) include singly and doubly diffracted rays and take into account slope diffraction contributions.

trends brought out above are fully representative for other angles of incidence.

Shadowed region [$\approx 160°, 180°$]

Without slope diffraction, the UTD yields a null field in the shadow region. This crude approximation can be improved upon by including slope diffraction terms. Figure 10 shows the comparison between the $MoM(D)$, $MoM(Zv)$ and $D12Maliu$ results where $D12Maliu$ denotes the UTD Maliuzhinets solution calculated using singly and doubly diffracted rays and including slope diffraction. In

the deep shadowed region [170°, 180°], the trends are almost the same as those observed for diffracted rays fields in the illuminated region. Near the shadow boundary, i.e., in [160°, 170°], errors in Maliuzhinets results are mainly due to a failing of the UTD. In comparison with the illuminated region results, the errors are:

- roughly of the same order of magnitude when the results are compared as diffracted rays fields,
- of much more important magnitude when the results are compared as total fields.

For urban channel modelling, we cannot state that such situations of overlapping transition zones may be considered as exceptional. Therefore, this deficiency of the UTD may have an important negative impact on the accuracy of predictions. Nevertheless, in default of a known efficient remedy for the problem of overlapping transition zones, including slope diffraction terms seems to be a not so bad makeshift solution.

Finally, in this application of the UTD to square cylinders, we have found that the computational time (CPU) increases twofold in going from the Luebbers coefficient to the Maliuzhinets one. In models of the urban channel, the step which consumes the main CPU time is by far the ray tracing computation. We conclude that there is no significant difference in CPU times between the two considered solutions.

5. SYNTHESIS AND CONCLUSION

Keeping beside CPU times and easiness to implement, i.e., considering only accuracy, we made evident that the best tendencies are indubitably obtained for the (Maliuzhinets/HF IBC) solution. However, bearing in mind all the imperfections embedded in urban channel models, we cannot state with objectivity that the other solutions are inadequate. Indeed, owing to—the dispersion of the urban material characteristics ($\bar{\varepsilon}$, $\bar{\mu}$)—the uncertainty of their actual values—surface roughness ...—, a single effective value for (ε, μ) is generally assumed in models. Thus, with the results of our simulations, it seems that the distinction between HI IBC and HF IBC is rather illusory and irrelevant. Moreover, when the 'preponderant forward and/or near shadow boundary diffractions' assumption is set forth, the Luebbers (modified formulation) and Maliuzhinets results become indistinguishable. In this case, the less cumbersome Luebbers' solution turns to be the better suited one. For this last assertion, the ability to include slope diffraction terms is kept away; it should be observed that anyhow all models burke fundamentally the problem of overlapping transition zones (grazing incidence).

Luebbers or Maliuzhinets solution with HF or HI IBC in urban channel models? It seems from the presented results that the answer is likely nothing than a matter of personal and subjective opinion.

APPENDIX A.

h function

The function h is defined in terms of the more standard Fresnel function $F_-(\nu)$ which is available in most of the subroutine's libraries:

$$F_-(\nu) = \int_{\nu}^{+\infty} \exp(-j\,t^2)\,dt \tag{A1}$$

This function h depends on one real variable Φ and two real parameters $(kL,\ N)$. It is simply denoted by $h(\Phi)$ and is defined as:

$$h(\Phi) = -\sqrt{kL}\,K_-(\nu)\Lambda \tag{A2}$$

where, with the use of the two auxiliary variables:

$$X = \frac{\Phi+\pi}{2N}, \quad \varepsilon = X - \mathrm{Nint}\left(\frac{X}{\pi}\right)\pi \quad (\mathrm{Nint}:\ \textit{Nearest integer}), \tag{A3}$$

the expressions of $\nu,\ \Lambda$ and $K_-(\nu)$ are given by:

$$\nu = \sqrt{kL}\,|\sin(N\varepsilon)| \tag{A4}$$

$$\Lambda = \frac{|\sin(N\varepsilon)|}{N}\,\cot(X) \tag{A5}$$

$$\left[= sign(\varepsilon)\left(1 - \left(\frac{N^2+2}{6}\right)\varepsilon^2\right) + O(\varepsilon^4) \text{ when } \varepsilon \to 0\right]$$

$$K_-(\nu) = \frac{1}{\sqrt{\pi}}\,\exp(j(\nu^2+\frac{\pi}{4}))F_-(\nu) \tag{A6}$$

$$\left[\begin{array}{l} K_-(\nu) = \dfrac{1}{2\nu\sqrt{j\pi}}\left(1 + \dfrac{j}{2\nu^2} + O\dfrac{1}{\nu^4}\right) \text{ when } \nu \gg 1 \\ K_-(0) = \dfrac{1}{2} \end{array}\right]$$

In these last equations, some useful equivalent asymptotic expansions are given into square brackets.

The main useful properties of $h(\Phi)$ are:

1. $h(\Phi + 2N\pi) = h(\Phi)$

2. For $\nu \gg 1$: $h(\Phi) \approx \dfrac{-1}{2N\sqrt{2j\pi}} \cot(X)$ (independant of kL)
3. For $\nu \to 0$: $h(\Phi) \approx -\dfrac{1}{2} sign(\varepsilon)\sqrt{kL}$ (at fixed kL)

For $\nu > \nu_c$ where $\nu_c \approx 3$, the property 2. gives an excellent approximation of $h(\Phi)$. When applied to the wedge diffraction problem, $\varepsilon = 0$ corresponds to one of the shadow boundaries; the angle $\alpha = 2N\varepsilon$ gives the direction of the field point measured from the shadow boundary $\varepsilon = 0$ with $\alpha < 0$ in the shadowed side.

hs function

The function hs is used to calculate slope diffraction coefficients. It is defined in terms of h derivative as:

$$hs(\Phi) = -jh'(\Phi). \tag{A7}$$

With the use of the two complementary variables:

$$d\nu = sign(\varepsilon)\sqrt{\frac{kL}{2}}\cos(N\varepsilon), \tag{A8}$$

$$\Gamma = \frac{\cot(N\varepsilon)}{2} - \frac{1}{N\sin(2X)} \tag{A9}$$
$$\left[= -\varepsilon\left(\frac{N^2+2}{6N}\right) + O(\varepsilon^3) \text{ when } \varepsilon \to 0\right],$$

$hs(\Phi)$ can be expressed as:

$$hs(\Phi) = \Lambda\sqrt{kL}\left(K_-(\nu)(j\Gamma - 2\,\nu\,d\nu) - j\sqrt{\frac{j}{\pi}}\,d\nu\right). \tag{A10}$$

The main useful properties of $hs(\Phi)$ are:

1. $hs(\Phi + 2N\pi) = hs(\Phi)$
2. For $\nu \gg 1$: $hs(\Phi) \approx -\dfrac{1}{4}\sqrt{\dfrac{j}{2\pi}}\left(\dfrac{1}{N\sin(X)}\right)^2$ (independant of kL)
3. For $\nu \to 0$: $hs(\Phi) \approx \dfrac{kL}{\sqrt{j2\pi}}$ (at fixed kL)

REFERENCES

1. Rossi, J. P. and A. J. Levy, "A ray model for decimetric radiowave propagation in an urban area," *Radio Science,* Vol. 27, No. 6, 971–979, 1992.
2. Lebherz, M., W. Wiesbeck, and W. Krank, "A versatile wave propagation model for the VHF/UHF range considering three-dimensional terrain," *IEEE Trans. Ant. Prop.,* Vol. AP-40, No. 10, 1121–1131, 1992.
3. Kürner, T., D. J. Cichon, and W. Wiesbeck, "Evaluation and verification of the VHF/UHF propagation channel based on a 3-D-wave propagation model," *IEEE Trans. Ant. Prop.,* Vol. AP-44, No. 3, 393–404, 1996.
4. Luebbers, R. J., "Finite conductivity uniform GTD versus knife edge diffraction in prediction of propagation path loss," *IEEE Trans. Ant. Prop.,* Vol. AP-32, No. 1, 70–76, 1984.
5. Luebbers, R. J., "Comparison of lossy wedge diffraction coefficients with application to mixed path propagation loss prediction," *IEEE Trans. Ant. Prop.,* Vol. AP-36, No. 1, 1031–1034, 1988.
6. Luebbers, R. J., "A heuristic UTD slope diffraction coefficient for rough lossy wedges," *IEEE Trans. Ant. Prop.,* Vol. AP-37, No. 2, 206–211, 1989.
7. Kouyyoumjian, R. G. and P. H. Pathak, "A uniform geometrical theory of diffraction for an edge in a perfectly conducting surface," *Proc. IEEE,* Vol. 62, No. 11, 1448–1461, 1974.
8. Tiberio, R., G. Pelosi, and G. Manara, "A uniform GTD formulation for the diffraction by a wedge with impedance faces," *IEEE Trans. Ant. Prop.,* Vol. AP-33, No. 8, 867–873, 1985.
9. Tiberio, R., G. Pelosi, G. Manara, and P. H. Pathak, "High-frequency scattering from a wedge with impedance faces illuminated by a line source, Part I: diffraction," *IEEE Trans. Ant. Prop.,* Vol. AP-37, No. 2, 212–217, 1989.
10. Bergljung, C. and L. G. Olsson,"A comparison of solutions to the problem of diffraction of a plane wave by a dielectric wedge," *IEEE Ant. and Prop. Society International Symposium,* 1992 Digest, Vol. 4, 1861–1864.
11. Demetrescu, C, C. C. Constantinou, and M. J. Mehler, "Scattering by a right-angled lossy dielectric wedge," *IEE Proc.-Microw. Antennas Propag.,* Vol. 144, No. 5, October 1997.
12. Leontovich, M. A., "Approximate boundary conditions for the electromagnetic field on the surface of a good conductor,"

Investigations on radiowave propagation, Part II, Moscow, Academy of Sciences, 1948.

13. Senior, T. B. A., "Approximate boundary conditions," *IEEE Trans. Ant. Prop.,* Vol. AP-29, No. 5, 826–829, 1981.
14. Senior, T. B. A., "Approximate boundary conditions for homogeneous dielectric bodies," *J. of Electromagn. Waves and Appl.,* Vol. 9, No. 10, 1227–1239, 1995.
15. Huddleston, P. L., "Scattering by finite, open cylinders using approximate boundary conditions," *IEEE Trans. Ant. Prop.,* Vol. AP-37, No. 2, 253–257, 1989.
16. Wang, D.-S., "Limits and validity of the impedance boundary condition on penetrable surfaces," *IEEE Trans. Ant. Prop.,* Vol. AP-35, No. 4, 453–457, 1987.
17. James, G. L., *Geometrical Theory of Diffraction for Electromagnetic Waves,* 3rd Edition, Peter Peregrinus Ldt., London, United Kingdom, 1986.
18. Aïdi, M. and J. Lavergnat, "Approximation of the Maliuzhinets function," *J. of Electromagnetic Waves and Applications,* Vol. 10, 1395–1411, 1996.